2017

System Identification of Motion Artifact: Noise in EEG Headsets from Locomotion

Kaela Shea
University of Waterloo, Canada, kshea@uwaterloo.ca

James Tung
University of Waterloo, Canada, james.tung@uwaterloo.ca

Recommended Citation

Shea, K. & Tung, J. (2017). System identification of motion artifact noise in EGG headsets from locomotion. *H-Workload 2017: The first international symposium on human mental workload, Dublin Institute of Technology, Dublin, Ireland, June 28-30. doi:10.21427/D75349 isbn:9781900454637 (vol)*

System Identification of Motion Artifact Noise in EEG Headsets from Locomotion

Kaela Shea[1] and James Tung[1]

University of Waterloo, Department of Mechanical and Mechatronics Engineering, Waterloo ON N2L 3G1, Canada*
kshea@uwaterloo.ca, james.tung@uwaterloo.ca

Abstract. Fall prevention for geriatric populations is a growing concern among clinicians and researchers due to severe risk of morbidity and loss of independence. Emerging evidence has demonstrated that mental workload while walking influences gait stability and the risk for falling. Electroencephalography (EEG) presents a potential method to provide objective measures of mental workload, particularly during daily activities. Noise introduced to the EEG signal during motion, however, is restrictive. The study presented in the following paper isolates EEG signal noise attained from gait for a commercially accessible EEG system, the Emotiv. Time and spectral system identification techniques were applied to model motion-induced artifacts given head linear and angular movement data. During gait of varying speeds (1.4-5.8 km/h), frequency and time domain system identification techniques were unable to accurately model the relationship between head movement and EEG signal noise with accuracies between 1% and 11% fit. However, analysis of data obtained during activities eliciting higher amplitudes of head movement (i.e., double-footed jumping) resulted in a high accuracy in linear system modelling, ranging from 68% to 74% fit, suggesting a dead-zone nonlinearity. Isolated EEG noise signals provide a ground truth measurement of the Emotiv system to estimate signal to noise ratio (SNR). Results of the SNR determined that, during gait, EEG signals are 8 to 20 times the power of gait-induced noise providing confidence in EEG recordings during ambulatory monitoring.

Keywords: EEG, System Identification, Motion, Geriatric Assessment, Ambulatory Monitoring

1 Introduction

Falls are a major risk of morbidity for elderly individuals and are severely detrimental to their independence [1]. Not only are falls more dangerous to the elderly, but impairments in cognition, balance, muscle strength, and sensory inputs all

* Research supported by the National Sciences and Engineering Research Council of Canada (NSERC)

contribute to an increased risk of falling in the geriatric population [2]. An estimated 30% of individuals aged 65 years and older experience at least one fall each year, a rate which increases with age [3]. As falls have the potential to drastically limit an individual's independence, the impact is felt throughout a community in an increased demand in caregiving. While awareness of falls among geriatric populations continues to gain traction with researchers and clinicians, preventative measures still receive relatively little clinical attention. The main barriers to effective intervention to potential falls in the elderly population are time and knowledge deficits in health care providers [2].

Research examining fall prevention programs have demonstrated moderately effectiveness. A review of the literature yielded 60 randomized control trials supporting the effectiveness of health-care based, and community based, fall prevention programs [2], further supported by cost-benefit economic analyses [4]. There are many strategies for fall prevention including: education, modification of the home environment, and physical training [5]. Interventions that utilize individualized assessments to target key risk(s) has proven to be the most effective within community based fall prevention programs ([2], [6]). A common protocol in fall prevention techniques involve identifying risk factors, assessing levels of risk, and implementation of an individualized prevention plan [7]. While assessment tools are accurate and sensitive, individualized assessment and planning are time consuming and resource intensive ([5],[7]). To reduce assessment burden on clinicians, technology has been leveraged to provide more sensitive tools.

Recently, cognitive deficits have been associated with an increased risk for falls. Numerous studies have demonstrated an interdependence between gait instability and cognitive impairment in older adults [1]. For example, Iersel et al. [8] demonstrated the relationship between performance on working memory tasks and reduced gait stability. Gait becomes an increasingly challenging activity, demanding more of the mental resources that diminishes due to aging ([9], [10], [11]). Mental workload describes the amount neural processing power, or cognitive resources, required for successful performance of a given task. Cognitive theory posits there is limited capacity for executive functioning, such as working memory and the ability to process novel information ([12], [13]). As elderly individuals must dedicate more mental workload resources to the action of maintaining a stable gait, additional tasks may negatively impact gait performance (i.e., dual-tasking) ([9], [11]). While previous research examining dual-task effects have focused on sensitive gait performance metrics (e.g., step time variability), complementary methods to measure levels of mental workload are few.

To address the need for more sensitive metrics of mental workload to assess fall risk, electroencephalography (EEG) presents a potential method [14]. Briefly, EEG measures electrical activity associated with neurocognitive function through electrodes applied to the scalp to capture a summation of post synaptic potentials across a broad neural area [13]. This neurophysiological technique allows for movement of the participant, as the subject is restricted only by light weight electrodes and miniaturized amplifiers [15]. The high temporal resolution of the EEG allows immediate neurological reactions to stimuli to be recorded. Based

on existing literature, oscillatory frequency information of the EEG signal can provide insight into the functional networks of the cortex as a defined range of frequencies are correlated with specific brain activities[13]. The adult human brain is capable of five distinct frequency bands: Delta, Theta, Alpha, Beta, and Gamma. The two spectra relevant for measurement of mental workload using EEG technology are Theta (4-7 Hz) and Alpha (7- 13 Hz), measured primarily at the dorsolateral prefrontal cortex ([13],[16]). Studies measuring Alpha and Theta waves using EEG technology demonstrate decreases in Alpha band power and increases in Theta band power during increasingly challenging working memory tasks, with strong reliability in measuring mental workload ([17],[13]).

While traditional EEG systems are resource-intensive and require long setup times, recent commercialization of EEG headsets have provided a promising alternative to acquire EEG signals ([18],[19]). A key feature is the use of convenient saline electrodes mounted to an adjustable headset, significantly reducing time required to prepare gel electrodes in traditional EEG systems. Lin et al. [20] successfully measured steady state evoke potentials using the Emotiv system during treadmill walking that mimics day-to-day gait. Furthermore, Duvinage et al. [21] evaluated the intrinsic performance of the Emotiv headset relative to a research grade ANT Waveguard system. While the researchers concluded that Emotiv performance proved acceptable, the study found that the medical grade system did significantly outperform the Emotiv during motion [21]. Our lab proposes using a commercially available EEG system, the Emotiv, to measure mental workload during daily routines as part of a wearable fall risk assessment system. By directly measuring workload in daily life, individuals may be assessed for specific activities that contribute to high mental workload levels and increase their risk of falling. This detailed information can be used to identify individual risks and generate intervention prevention targets.

Despite the potential of commercial EEG technology for attaining a new perspective on mental workload recording, constraining factors limit the use of EEG systems outside of a research lab. In particular, motion artifacts restrict the acquisition of sufficiently high quality signals [22]. Motion artifacts in EEG are difficult to identify and obscure neural information. Many simple artifact removal techniques result in the degradation of the quality of signals of interest [23]. Even powerful signal processing tools such as Blind Source Separation, including Independent Component Analysis (ICA), are associated with high computational expense and cannot reliably mitigate noise induced through full body motion ([24], [23]).

An extensive review of methods for the detection and removal of artifacts from scalp EEG revealed no universally accepted artifact detection or rejection technique [23]. Identifying the characteristics of artifacts remains the most important step in mitigating their influence on signals. However, in absence of ground truth motion artifact data in literature, popular methods for removing EEG artifacts rely on estimating the influence of poorly characterized artifacts in data [23]. Oliveira et al [24] stated the influence of motion on EEG must be recorded directly to develop sufficient understanding of the corrupting artifact. Head move-

ment during gait has been well-examined with the strongest correlation found in the vertical axis of motion ([25], [26]). Oliveira et al. [24] attempted to model motion artifact using a phantom head model on a robotic arm to induce vertical displacement. However, examination of motion artifact from actual human motion remains underexamined.
Using a novel human paradigm, Kline et al. investigated motion artifacts introduced through gait [27]. Physiological signals were blocked using a silicone swim cap such that electrodes of the EEG cap recorded only motion artifact. Using an accelerometer was incorporated into the system to measure head acceleration, regression techniques were applied to create a linear model relating head movement and motion artifact [27]. However, the authors concluded walking speed and did not yield a strong linear relationship to head acceleration.

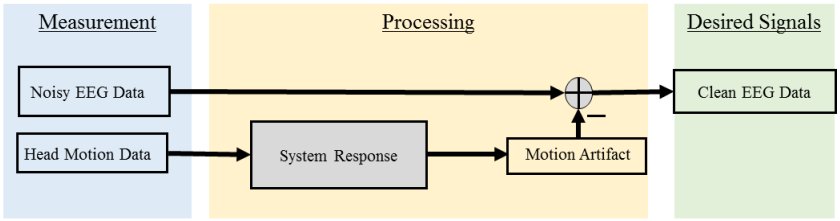

Fig. 1. Model of proposed signal processing technique

The current paper describes a study aiming to model gait-induced motion artifact using head acceleration by applying time- and frequency-based system identification techniques. We aim to simulate an accurate representation of the EEG motion artifact, as represented in Figure 1, given head motion data to facilitate artifact removal techniques. Our research studied a commercially available EEG headset, the Emotiv. We hypothesize that the motion artifact recorded using the swim cap paradigm can be predicted from head acceleration and angular velocity during movement.

2 Materials and Methods

2.1 Materials

The Emotiv EPOC+, produced by Emotiv Inc, is a wireless headset measuring EEG signals at 14 different electrode sites; AF3, F7, F3, FC5, T7, P7, O1, O2, P8, T8, FC6, F4, F8, AF42 (see Figure 2). For recording, the Emotiv EPOC+ does not require conductive gel and increases conductivity of the electrode-skin interface through felt pads soaked in saline solution and secured to the electrodes. Raw EEG data is collected from the Emotiv EPOC+ using software produced by Emotiv Inc.; Emotiv Xavier Pure [18].

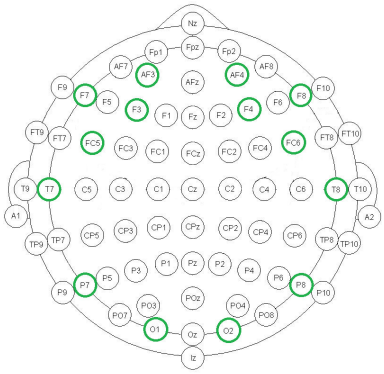

Fig. 2. Layout of Emotiv electrode position

The Emotiv EEG measurement system records tri-axial acceleration with an IMU built into the device [18]. A summary table of Emotiv technical specifications can be found below (see Table 1).

Table 1. Summary of technical specifications of the EEG capture system

Technical Specifications	Emotiv System
IMU Signals	3D accelerometer, 3D gyroscope, 3D magnetometer
IMU Sampling Rate	64 Hz
Number EEG of Electrodes	14
EEG Sampling Rate	128 Hz
Data Transmission	2.4 GHz wireless band
Resolution	14 bit
Signal Bandwidth	0.2 - 43 Hz
Built in Filters	5th order Sinc
	50 Hz and 60 Hz notch
Battery Life	12 hours

2.2 Experimental Setup

Seven healthy young adults, ages 18-25 volunteered to participate in our study. Measurements of head size, which influences the fit of Emotiv headset, and height, which influences gait, were taken. Due to the application of the swim cap as described below, hair thickness variability between participants will not influence data. Refer to Table 2 for physiological characteristics of all the participants. To ensure a typical representation of gait, participants were screened for musculoskeletal injuries and experiencing pain or discomfort during movement.

Participants were also free of lacerations, abrasions, and contusions on their head due to the potential discomfort arising from contact with the silicone swim cap. Participants self-reported any condition that would exclude them from the study.

Table 2. Participant descriptive characteristics

Study No.	**Head Circumference** (cm)	**Nasion - Inion** (cm)	**Height**(cm)
1	60	40	185
2	57	35	170
3	62	40	168
4	59	34	165
5	61	39	173
6	58	36	185
7	56	34	165

Following the protocol introduced by Kline et al. [27], a silicon swim cap was used to insulate neural signals from the EEG measurement device. To simulate the conductivity of human skin, the silicone swim cap was wrapped with cotton gauze saturated with conductive gel. Conductivity of the gel soaked gauze was measured using a digital multimeter, gel application was adjusted to ensure the measured conductivity was within the range of dry human skin (0.001-0.1 MΩ) [27]. Emotiv headset was otherwise set up normally per manufacturer's use instructions [18]. In the absence of actual neural signals, the electrodes recorded only signal artifacts [27].

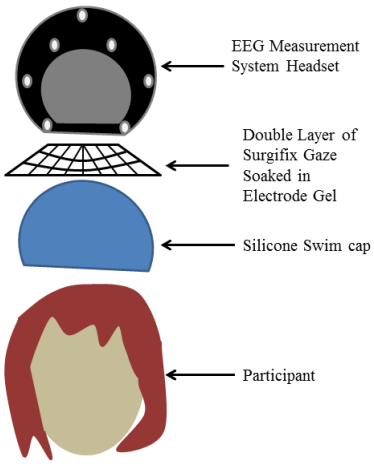

Fig. 3. Illustration of experimental set up

2.3 Data Collection Task

Participants were asked to walk on a treadmill with no incline at set speeds for five minutes. Walking speeds were presented at random order and ranged from very slow to a brisk pace. The four speeds participants walked at were: 1.4 km/h, 2.9 km/h, 4.32 km/h and 5.86 km/h, each speed is defined as a separate trial during the data collection session. At the start of each trial, prior to initiating the treadmill speed, patients performed three double footed jumps. The purpose of the jumps was to clearly segment each trial, and to synchronize pressure insoles worn by the participant (not used in the current study). After a walking trial of 5 minutes, the treadmill was stopped and the participant performed another set of five double footed jumps.

2.4 Data Processing and Analysis

Collected EEG and head motion data were processed offline using MathWorks' MatLab R2016a [28]. Each trial was segmented into individual trials (4 trials corresponding to the different walking speeds). Using a least squares filter design tool from MatLab, a 4-15 Hz bandpass finite impulse response (FIR) filter was applied to EEG signals (focusing on Alpha and Theta frequencies).
Cross correlation was performed to evaluate which motion signal best represented the energy of the noise data obtained from the electrodes. In performing cross-correlation of each X,Y, and Z axes of the accelerometer and gyroscope data between each electrode channel data, the Y axis accelerometer consistently yielded the highest correlations. Supported by previous research reporting similar observations [26], Y axis acceleration was used for the rest of data analysis to represent head movement.
Motion induced artifact and head movement data were then detrended to remove offsets introduced through filtering. We employed time and frequency domain system identification techniques to model the introduction of motion artifact into EEG measurements.

Time Domain Analysis. The impulse response function (IRF) provides insight into structure of a system as the time domain representation of a system transfer function [29], [30]. Let $h\,(i)$ represent an IRF such that a linear system is represented by

$$y\,(t) = \Delta t \sum_{t=0}^{T} h\,(i)\,u\,(t-i) \tag{1}$$

where u and y represent the discrete input and output signals, respectively.
The IRF, as defined in Equation 1, provides a mathematical representation for analysis of the relationship between movement and noise. In the current study, a correlational approach was used to estimate the IRF through the use of the System Identification Toolbox in MatLab [28].

Time–Frequency Domain Analysis. Due to the periodic nature of the gait cycle, head motion and motion artifact attained during gait are non-stationary signals and simple time and frequency representations may be unlikely to accurately represent the system response [23]. Furthermore, nonlinear relationships may also hinder accurate IRF estimation. To address these limitations, time resolution wavelets provided in frequency analysis were utilized.

The wavelet transform provides an advantage over time domain system identification techniques in the ability to model non-linearities [31]. Defined in Equation 5, the wavelet transform provides information with respect to a signal $x(t)$ at various time resolutions. This is accomplished by decomposing a signal into various orthogonal wavelets that are derived from a mother wavelet that is shifted in time and scale [32]. In Equations 2 through to 7, s represents the scale factor of the wavelet, and τ represents the time location of the wavelet. There are many different mother wavelet forms. In our analysis we chose a Morlet Wavelet that is characterized as a symmetric impulse as many signals and artifacts produced through mechanical dynamics of movement and vibration can be represented by impulses [32]. The Morlet Wavelet is defined in Equation 2.

$$\psi_{s,\tau}(t) = \exp(\frac{-\beta^2(t-\tau)^2}{s^2})\cos(\frac{\pi(t-\tau)}{s}) \tag{2}$$

$$As\ \beta \to 0\ \ \psi_{s,\tau}(t) \approx \cos(\frac{\pi(t-\tau)}{s}) \tag{3}$$

$$As\ \beta \to \infty\ \ \psi_{s,\tau}(t) \approx \delta(x)\ \ . \tag{4}$$

β defines the shape of the wavelet and acts as a balance between resolutions of time and frequency. As β tends to 0 the Morlet Wavelet resembles a cosine function, offering high frequency resolution at the expense of no time resolution. Conversely as β tends to ∞ the Morlet Wavelet resembles a dirac impulse function that offers high time resolution at the expense of no frequency resolution [32].

$$\mathscr{W}\psi, s, \tau = \langle \psi_{s,\tau}(t), x(t) \rangle = |s|^{-\frac{1}{2}} \int x(t)\psi^*_{s,\tau} dt\ \ . \tag{5}$$

To attain a time-frequency representation of the relationship between motion artifact and head acceleration, the magnitude wavelet coherence was calculated. Wavelet coherence is a measure of correlation between two signals and evaluates the degree of coherence and phase relation at each frequency scale. It is defined in Equation 8 as the function of power cross spectral density, defined in Equation 7, and the power spectral densities, defined in Equation 6. The Magnitude Squared Wavelet Coherence measures, at each point in time, the amount of energy in similar frequencies between two signals [31].

$$\mathscr{P}_{\psi,s,\tau}\{x(t)\} = \mathscr{W}_{\psi,\mathbf{s},\tau}\{x(t)\} * \mathscr{W}^*_{\psi,\mathbf{s},\tau}\{x(t)\} = |\mathscr{W}_{\psi,\mathbf{s},\tau}\{x(t)\}|^2 \tag{6}$$

$$\mathscr{X}_{\psi,s,\tau}\{x(t), y(t)\} = \mathscr{W}^*_{\psi,s,\tau}\{x(t)\} * \mathscr{W}_{\psi,s,\tau}\{y(t)\} \tag{7}$$

$$\mathscr{C}_{\psi,s,\tau}\{x(t), y(t)\} = | \frac{(|\mathscr{X}_{\psi,s,\tau}\{x(t), y(t)\}|)}{(|\mathscr{P}_{\psi,s,\tau}\{x(t)\}\mathscr{P}_{\psi,s,\tau}\{y(t)\}|)^{\frac{1}{2}}} |^2\ \ . \tag{8}$$

Signal to Noise Ratio. The calculation of the signal to noise ratio (SNR) is a measure of the power of the neural signal relative to the power of the noise. It is calculated as the ratio of summed squared magnitude of signal, X, to that of the noise, K, measured in decibels.

$$\text{SNR} = 10 * \log_{10} \left(\frac{\sum_{n=1}^{N} X_n^2}{\sum_{n=1}^{N} K_n^2} \right) \quad . \tag{9}$$

The isolated noise data collected as described above (i.e., swim cap paradigm) was used to estimate noise levels. Estimates of the neural signal magnitude were calculated from previously collected data using the Emotiv system from 7 different healthy, young adult participants performing a memory task while sitting stationary (i.e., minimal motion artifact).

3 Results

Due to significance in measuring mental workload and relatively large signal magnitudes, electrode sites AF3 and AF4 will be highlighted in the Results. Positioned over the dorsolateral prefrontal cortex, AF3/4 has been associated through fMRI and FNIRS studies to produce the large changes in activity correlated with varying levels of mental workload [16]. Furthermore, signals isolating motion artifact acquired in the current study from AF3/4 were large compared to most other sites. Hence, we focus on identification results for these electrodes as a representative cases for all sites.

3.1 Analysis of Walking Trials

Time Domain Analysis. An estimate of a linear system relating head movement and motion artifact was generated by the impulse response function (IRF), calculated as in Equation 1. Fit of the IRF model was determined by comparing between predicted outputs using the IRF model and the measured outputs of the system (i.e., electrode noise) using Percentage Fit. Equation 10 describes the calcuation used where Ym is measured output, Ys is simulated output, and $\overline{Ym}$ is the mean of the measured output.

$$PercentageFit \ = 100 \left(1 - \frac{|Ym - Ys|}{|Ym - \overline{Ym}|} \right) \tag{10}$$

An IRF is estimated and evaluated for each electrode site of the Emotiv, for every trial of different speed, per participant. Table 3 summarizes the noise magnitude, percent fit, and SNR for each site at 4.3 km/h walking speed. Magnitude of the measured electrode noise is represented in the root mean squared (RMS) value at each site. Figure 4 allows for a visual comparisons between the measured and simulated signals of site AF3.

Table 3. Measured noise magnitude, percentage fit (see Equation 10) between the simulated and true system output, and signal to noise ratio (SNR) averaged across all participants at walking speed of 4.32 km/h

Site	AF3	F7	F3	FC5	T7	P7	O1	O2	P8	T8	FC4	F4	F8	AF4
Noise RMS	24.1	16.9	7.7	6.2	9.0	6.7	6.3	5.6	5.0	6.0	7.2	27.3	4.2	5.3
Percent Fit	9.0	3.6	6.3	7.9	4.1	3.3	1.1	2.1	4.8	5.8	4.3	3.9	5.7	6.1
SNR	20	12	10	13	17	9	11	-1	9	13	8	11	19	14
SNR SD	3	3	2	2	2	2	2	2	2	2	2	2	4	3

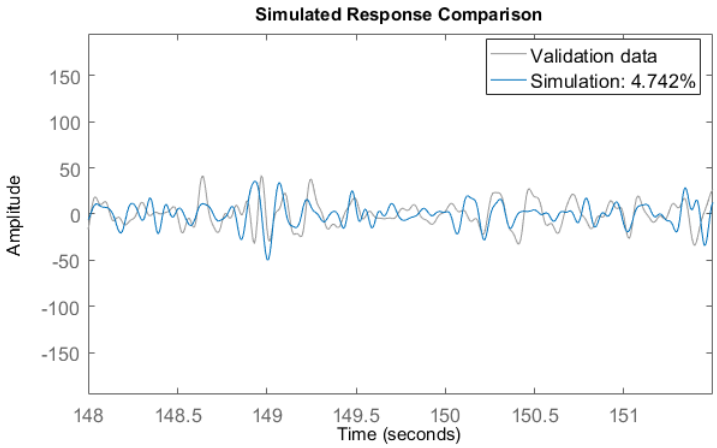

Fig. 4. Impulse response function (IRF) model simulation of electrode noise alongside measured electrode noise for site AF3 (4.742% fit)

In general, the linear IRF models yielded poor representations of the electrode noise measured during the walking trials indicated by low Percent Fit values displayed in Table 3. As a measure of the potential impact of the motion artifact noise associated with gait, SNR values indicate a high power of neural signal (measured from participants performing a memory task while stationary, see Signal to Noise Ratio section) relative to motion artifact (i.e., noise). As seen in Table 3, high signal magnitudes (8-20 times greater than noise levels) were observed consistently across all locations with the exception of the electrode position O2. Table 4 expands Table 3 results of sites AF3 and AF4 across all the time trials.

Table 4. Noise magnitude (RMS) and percent fit between the simulated and measured output averaged across all participants by walking speed for AF3 and AF4

Speed(km/h)	**AF3 Noise RMS**	**AF3 Percent Fit**	**AF4 Noise RMS**	**AF4 Percent Fit**
1.4	8.57	10.2	19.20	5.4
2.9	16.27	9.4	7.95	3.7
4.3	24.14	9.0	5.32	6.1
5.8	21.72	7.2	17.49	5.29

Time-Frequency Domain Analysis. Figure 5 exhibits the wavelet coherence magnitude, as defined in equations 2 to 8, between head motion measured during a gait speed of 4.3 km/h, and motion artifact measured at site AF3. The value of 1, denoted in Figure 5 by bright yellow, represents the strongest possible wavelet coherence between the two signals, while a value of 0, denoted by deep blue in Figure 5, denotes no coherence. A strong coherence indicates similar energy present in the signal occurring at the same frequency and phase[31]. As shown in Figure 5 there exists regions of strong coherence between the head motion and motion artifact signals in the low frequency range of approximately 0.02 Hz to 1 Hz at various periods of time.

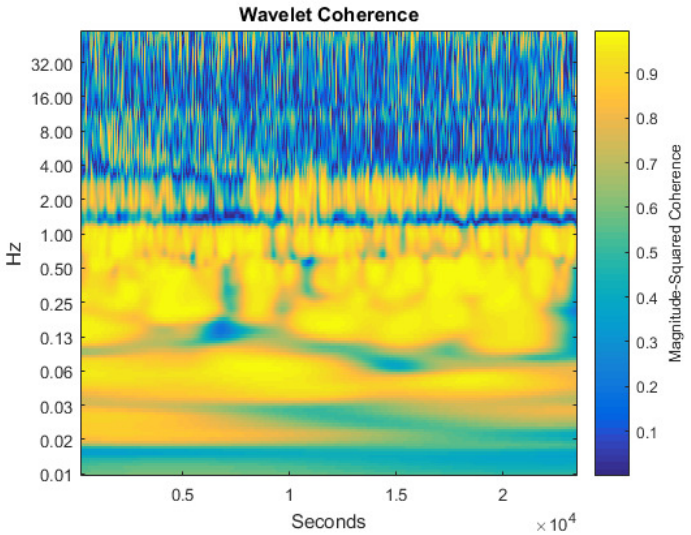

Fig. 5. Time varying wavelet coherence between motion induced artifact signal and z-axis head movement at a walking speed of 4.3 km/h at AF3

3.2 Analysis of Jumps

Periods at which high coherence between head motion and electrode noise were observed in Figure 5 corresponded to times of high head motion amplitude. Given this observation, we hypothesized a strong relationship between head motion and motion artifact only when motion exceeds a threshold (i.e., dead-zone). To test whether this type of nonlinear relationship exists, we chose to specifically examine data recorded during times of known increased head motion. For this we used data collected during the jumps participants performed, collected initially for the purpose of segmenting each trial.
Figure 6 plots the wavelet coherence magnitude, during a series of jumps, between head motion and electrode noise measured at electrode position AF3. It can be observed that high amplitude head movement elicits a high coherence with electrode noise in all frequency components in the period of jumps (between 1-2.5 seconds). Table 5 shows the Percentage Fit of the electrode noise simulation for every electrode site averaged across all the jumps of all the participants.

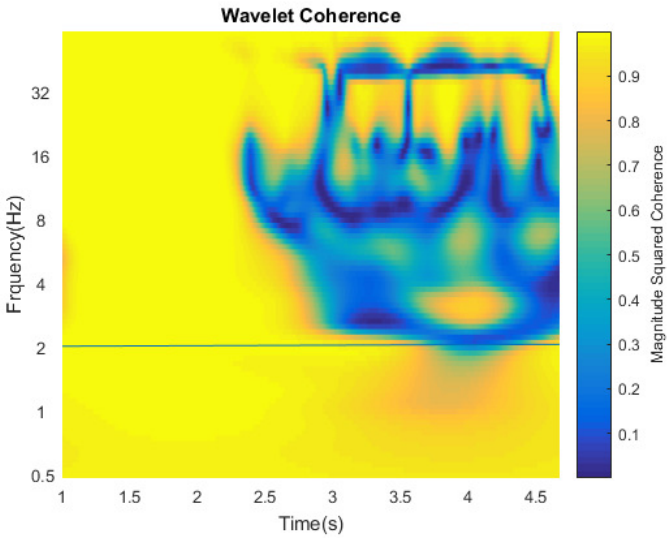

Fig. 6. Time varying wavelet coherence between AF3 site electrode motion induced artifact signal and z-axis head movement measured during a series of jumps

Using the jump data, IRFs were used to model and simulate electrode noise given the recorded head movement. Figure 7 provides a visual comparison between the measured and simulated noise signals of AF3 electrode position.

Compared to percent fits from the gait data (10.2% or less), the high amplitude motions yielded significantly more accurate simulations of electrode noise with little variance between electrode sites, as observed in Table 5.

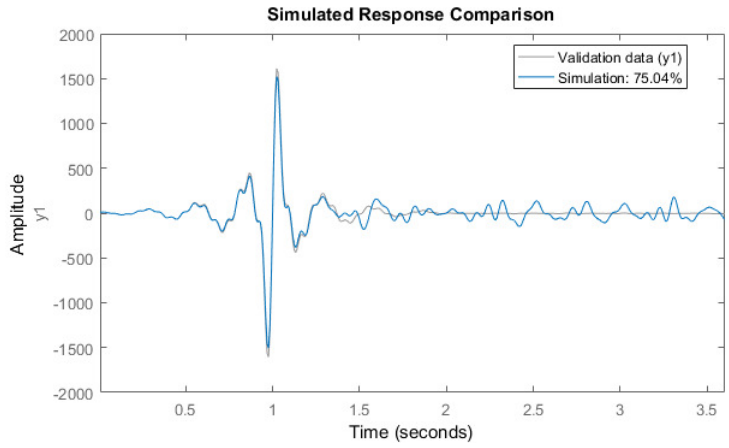

Fig. 7. Impulse response function (IRF) estimate of electrode noise alongside measured electrode noise for site AF3 during jumps (75.04% fit)

Table 5. Display of the Percentage Fit (see Equation 10) between the simulated and true system output averaged across all participants measured during participants performing jumps

Site	**AF3**	**F7**	**F3**	**FC5**	**T7**	**P7**	**O1**	**O2**	**P8**	**T8**	**FC4**	**F4**	**F8**	**AF4**
Percent Fit	73.6	71.7	71.6	72.2	67.8	70.7	71.3	74.3	71	71.8	71.8	71.8	71.9	72.4

4 Discussion

In this study, we hypothesized that motion artifact noise introduced to the EEG signal is the result of electrode motion in relation to the input of head movement. Using the protocol described above in Materials and Methods, motion artifact noise was isolated and collected from Emotiv electrodes using a swim cap paradigm. Head motion was measured using a 3D accelerometer built into the Emotiv device[18]. The z-axis of the accelerometer (i.e., vertical plane) was determined as the strongest influence to electrode noise, and was used to model head movement during gait.

Impulse response functions (IRF) were estimated to model the relationship between head movement and motion artifact measured by the Emotiv system during the walking trials, with poor results (no greater than 10.2% fit). The lack of ability to produce a linear model to accurately simulate motion artifact may be attributed to the non-linear nature of the signal.

Using a Time-Frequency analysis, the magnitude square coherence was calculated between electrode noise and head motion. Wavelet transforms are better suited for modelling non-linearities than the IRF method [33]. As such, results of the magnitude squared wavelet coherence, visually depicted in Figure 5, provide insight as to how the frequency and time components of noise relate to head

movement. We observed that head movement influenced noise greatest at low frequencies; below the 1 Hz frequency range. This finding may be attributed to the influence of body movement, as opposed to impact due to heel strike, as the primary origin of EEG motion artifact. Head movement was also shown to influenced noise greater in certain time regions.

In reviewing data to determine possible causes for coherence varying across time, regions of high coherence corresponded to regions of high amplitude accelerations. This was attributed to a non-linearity in the relationship between electrode noise and head movement of a dead-zone, indicating that head movement must be at a certain amplitude threshold before it is reflected in electrode noise. To examine this phenomenon further we analyzed data collected during a known region of high head movement amplitude: as participants performed jumps. Initially used as a method to segment walking trials, the jump data provided sufficient EEG and accelerometer recording of high amplitude head movement data. Displayed in Figure 6 coherence between electrode noise and head movement was greatly increased during the jumps relative to the coherence observed during walking trials. Furthermore the IRF system model was able to simulate electrode noise given head motion data with accuracies ranging between 68% to 74% as shown in Table 5. The success in modelling electrode noise using the IRF indicates that, with a certain amplitude of movement, electrode noise is linearly related to head motion. Based on these findings, future research to identify the threshold at which electrode noise linearly relates to head motion is warranted.

The data collection protocol used in this study allows for a measurement of EEG signals that are composed solely of system noise isolated from all neurophysiological signals. As there is no literature reporting ground truth data for noise of EEG systems, this noise data has potential to provide new insights into EEG signal processing [23]. Using the ground truth noise data of the Emotiv system affords estimates of the SNR attained by the Emotiv in measuring EEG signals at the frequencies relevant for measuring mental workload; 4Hz – 15Hz [13]. The SNR estimates show that EEG signals recorded from the Emotiv held 8 to 20 times the power of the noise level (Table 3). This high SNR result had the notable location exception of electrode O2, which consistently performed poorly. Due to the variance in head sizes and shapes between participants, it is unlikely that this location dependency is caused by the variance in pressure fit of the Emotiv headset.

The high SNR findings from this study support the potential use of the Emotiv system for measuring mental workload during ambulatory activities. In particular, the region with the most relevance to measuring mental workload is the dorsolateral prefrontal cortex that correspond to electrodes at positions AF3 and AF4 [16]. As shown in Table 3, SNR estimates are 20 and 14 for AF3 and AF4, respectively, strongly support the use of these sites to measure mental workload.

5 Conclusion

The time domain linear system identification of impulse response functions failed to provide an accurate model for simulating motion artifact introduced through head motion during walking. Electrode noise pertaining to regions of high movement amplitude were, however, modelled with a high accuracy using linear system identification. Forthcoming efforts will investigate the amplitude threshold of movement needed to achieve a linear relationship between head motion and EEG electrode noise. Using the obtained ground truth EEG signal noise data, SNR of the Emotiv system was calculated yielding high results in the location and frequencies relevant in measuring mental workload. In measuring mental workload during walking with the Emotiv headset, we are confident EEG signal noise arising from gait motion will not prove a significant limitation.

References

1. M. Montero-Odasso, J. Verghese, O. Beauchet, and J. Hausdorff, "Gait and cognition: A complementary approach to understanding brain function and the risk of falling," *Progress in Geriatrics*, 2012.
2. M. E. Tinetti, C. Gordon, E. Sogolow, P. Lapin, and E. H. Bradley, "Fall-Risk evaluation and management: Challenges in adopting geriatric care practices," *The Gerontologist*, vol. 46, pp. 717–725, Dec. 2006.
3. W. H. Organization, "WHO global report on falls prevention in older age," tech. rep., World Health Organisation, 2007.
4. M. R. C. Hendriks, S. M. A. A. Evers, M. H. C. Bleijlevens, J. C. M. van Haastregt, H. F. J. M. Crebolder, and J. T. van Eijk, "Cost-effectiveness of a multidisciplinary fall prevention program in community-dwelling elderly people: A randomized controlled trial (ISRCTN 64716113)," *International Journal of Technology Assessment in Health Care*, vol. 24, pp. 193–202, Apr. 2008.
5. M.-R. Lin, S. L. Wolf, H.-F. Hwang, S.-Y. Gong, and C.-Y. Chen, "A randomized, controlled trial of fall prevention programs and quality of life in older fallers," *Journal of the American Geriatrics Society*, vol. 55, pp. 499–506, Apr. 2007.
6. S. R. Lord, A. Tiedemann, K. Chapman, B. Munro, S. M. Murray, M. Gerontology, G. R. Ther, and C. Sherrington, "The effect of an individualized fall prevention program on fall risk and falls in older people: A randomized, controlled trial," *Journal of the American Geriatrics Society*, vol. 53, pp. 1296–1304, Aug. 2005.
7. P. Palumbo, L. Palmerini, S. Bandinelli, and L. Chiari, "Fall risk assessment tools for elderly living in the community: Can we do better?," *PLOS ONE*, vol. 10, pp. e0146247+, Dec. 2016.
8. M. B. van Iersel, R. P. C. Kessels, B. R. Bloem, A. L. M. Verbeek, and M. G. M. Olde Rikkert, "Executive functions are associated with gait and balance in Community-Living elderly people," *The Journals of Gerontology Series A: Biological Sciences and Medical Sciences*, vol. 63, pp. 1344–1349, Dec. 2008.
9. N. Theill, M. Martin, V. Schumacher, S. Bridenbaugh, and R. Kressig, "Simultaneously measuring gait and cognitive performance in cognitively healthy and cognitively impaired older adults: The basel Motor-Cognition Dual-Task paradigm," *Journal compilation the American Geriatrics Society*, 2011.

10. M. Mielke, R. Roberts, R. Savica, R. Cha, D. Druback, T. Christianson, V. Pankratz, Y. Geda, M. Machulda, R. Ivnik, D. Knopman, B. Boeve, W. Rocca, and R. Petersen, "Assessing the temporal relationship between cognition and gait: Slow gait predicts cognitive decline in the mayo clinic study of aging," *Journals of Gerontology*, 2013.
11. R. L. Smith-Ray, S. L. Hughes, T. R. Prohaska, D. M. Little, D. A. Jurivich, and D. Hedeker, "Impact of cognitive training on balance and gait in older adults," *Journals of Gerontology*, 2013.
12. K. K. Sreenivasan, C. E. Curtis, and M. DEsposito, "Revisiting the role of persistent neuralactivity during working memory," *Trends in Cognitive Sciences*, vol. 18, pp. 82–89, Feb. 2014.
13. P. Antonenko, F. Paas, R. Grabner, and T. van Gog, "Using electroencephalography to measure cognitive load," *Educational Psychology Review*, 2010.
14. P. De Sanctis, J. S. Butler, B. R. Malcolm, and J. J. Foxe, "Recalibration of inhibitory control systems during walking-related dual-task interference: A mobile Brain-Body imaging (MOBI) study," *NeuroImage*, 2014.
15. K. Gramann, D. P. Ferris, J. Gwin, and S. Makeig, "Imaging natural cognition in action," *International Journal of Psychophysiology*, 2013.
16. F. A. Fishburn, M. E. Norr, A. V. Medvedev, and C. J. Vaidya, "Sensitivity of fNIRS to cognitive state and load.," *Frontiers in human neuroscience*, vol. 8, 2014.
17. L. K. McEvoy, M. E. Smith, and A. Gevins, "Test-retest reliability of cognitive EEG," *lCinical Neurophysiology*, 2000.
18. E. Inc, "Emotiv EPOC+." `www.emotiv.com`, 2014. Online; accessed 20-November-2016.
19. R. Zink, B. Hunyadi, S. Van Huffel, and M. De Vos, "Mobile EEG on the bike: disentangling attentional and physical contributions to auditory attention tasks," *Journal of Neural Engineering*, vol. 13, June 2016.
20. Y.-P. Lin, Y. Wang, and T.-P. Jung, "Assessing the feasibility of online SSVEP decoding in human walking using a consumer EEG headset," *Journal of Neuro-Engineering and Rehabilitation*, 2014.
21. M. Duvinage, T. Castermans, M. Petieau, T. Hoellinger, G. Cheron, and T. Dutoit, "Performance of the emotiv epoc headset for p300-based applications," *BioMedical Engineering OnLine*, 2013.
22. A. S. Oliveira, B. R. Schlink, W. D. Hairston, P. Koing, and D. P. Ferris, "Proposing metrics for benchmarking novel EEG technologies towards Real-World measurements human neuroscience," *Froutiers in Human Neuroscience*, vol. 10, May 2016.
23. M. K. Islam, A. Rastegarnia, and Z. Yang, "Methods for artifact detection and removal from scalp EEG: A review," *Neurophysiologie Clinique/Clinical Neurophysiology*, vol. 46, pp. 287–305, Nov. 2016.
24. A. S. Oliveira, B. R. Schlink, W. D. Hairston, P. König, and D. P. Ferris, "Induction and separation of motion artifacts in EEG data using a mobile phantom head device," *Journal of Neural Engineering*, vol. 13, pp. 036014+, June 2016.
25. J. J. Kavanagh, S. Morrison, and R. S. Barrett, "Coordination of head and trunk accelerations during walking," *European Journal of Applied Physiology*, vol. 94, pp. 468–475, July 2005.
26. E. Hirasaki, S. T. Moore, T. Raphan, and B. Cohen, "Effects of walking velocity on vertical head and body movements during locomotion," vol. 127, no. 2, pp. 117–130, 1999.

27. J. E. Kline, H. J. Huang, K. L. Snyder, and D. P. Ferris, "Isolating gait-related movement artifacts in electroencephalography during human walking.," *Journal of neural engineering*, vol. 12, Aug. 2015.
28. MathWorks, "MathWorks - makers of MATLAB and simulink - MATLAB & simulink." `https://www.mathworks.com/`, 2016. Online; accessed 22-December-2016.
29. I. W. Hunter, R. E. Kearney, and L. A. Jones, "Estimation of the conduction velocity of muscle action potentials using phase and impulse response function techniques," *Medical and Biological Engineering and Computing*, vol. 25, pp. 121–126, Mar. 1987.
30. D. T. Westwick and R. E. Kearney, "Identification of physiological systems: a robust method for non-parametric impulse response estimation," vol. 35, no. 2, pp. 83–90, 1997.
31. D. Chinarro, *System Engineering Applied to Fuenmayer Karst Aquifer (San Julian de Banzo, Huesca) and Collins Glacier (King George Island, Antarctica)*. Springer International Publishing, 2014.
32. J. Lin and L. Qu, "Feature extraction based on morlet wavelet and its application for mechanical fault diagnosis," *Journal of Sound and Vibration*, vol. 234, pp. 135+, Jan. 2000.
33. J. B. Thomas, "Using the coherence function as a means to improve frequency domain least squares system identification," Master's thesis, Russ College of Engineering and Technology of Ohio University, Mar. 2007.